Hydrogen and Deuterium Atoms in Octasilsesquioxanes: Experimental and Computational Studies

ARTICLE *in* JOURNAL OF THE AMERICAN CHEMICAL SOCIETY · JUNE 2006

Impact Factor: 12.11 · DOI: 10.1021/ja055177d · Source: PubMed

3 AUTHORS, INCLUDING:

Michael Päch
Up Transfer GmbH
20 PUBLICATIONS **176** CITATIONS
SEE PROFILE

Roderick Macrae
Marian University
67 PUBLICATIONS **348** CITATIONS
SEE PROFILE

J|A|C|S
ARTICLES
Published on Web 04/14/2006

Hydrogen and Deuterium Atoms in Octasilsesquioxanes: Experimental and Computational Studies

Michael Päch,† Roderick M. Macrae,*,‡ and Ian Carmichael

Contribution from the Radiation Laboratory, University of Notre Dame, Notre Dame, Indiana 46556

Received August 14, 2005; E-mail: rmacrae@marian.edu

Abstract: The rate of detrapping of atomic hydrogen from several octasilsesquioxanes is the same for dissolved and solid samples and is independent of the presence of other species such as free radicals or oxygen; varying the cage substituents leads to only minor differences in the activation parameters. Hydrogen atoms are found to be more strongly stabilized in homosubstituted octasilsesquioxanes compared with singly Ge-substituted cages. A kinetic isotope effect observed for the detrapping of H and D from MeT_8 is ascribed to the difference in the zero-point energies of the trapped atoms. There is a secondary H/D isotope effect in the temperature dependence of the ^{29}Si-superhyperfine splitting constants in the range 228−353 K. Cage relaxation has a substantial effect on the detrapping barrier but little influence on the intracage potential. Calculations using a rigid cage approximation give satisfactory agreement with zero-point parameters extracted from experimental data. Different model chemistries yield qualitatively different pictures of the dependence of the hyperfine coupling constant of the trapped H atom upon the detrapping coordinate. Within an isotropic approximation of the vibrational displacements, the B3LYP data give fairly close agreement with the experimental temperature dependence, subject to a shift of the absolute value related to known weaknesses of the method. For the Si_7Ge cage, it is found that the transition state in which the H atom passes through a Ge-containing face is strongly favored, accounting for the larger detrapping rate parameters observed experimentally for this species.

Introduction

Single atoms and few-atom-ensemble species noncovalently confined in closed structures have received considerable attention in recent years. These so-called endohedral systems not only pose challenging experimental problems in themselves but also create possibilities for sensitive testing grounds of advanced quantum chemical methods. Although muonium (Mu) in C_{60}[1] and RT_8[2] (RT_8 indicates a homosubstituted octa(alkylsilsesquioxane—i.e., $R_8Si_8O_{12}$, where R denotes the alkyl substituent) provide more exotic examples, endohedral fullerenes are by far the more prominent members of this class of compounds. They have been produced by methods as different as electrothermal vaporization (ETV) of metal-impregnated graphite rods in a Kroto-type device,[3] ETV of graphite in a helium atmosphere, thermal implantation of noble gases into C_{60},[4,5] and low-energy ion implantation in the case of nitrogen and phosphorus atoms.[6]

The last of these methods, first applied by Weidinger et al. to fullerenes,[7] proved successful also for filling the central Si_8O_{12} units of octasilsesquioxanes with H and D atoms.[8] In an evacuated cell, the encaging molecules (C_{60}, C_{70}, different RT_8's) are sublimed onto a cooled copper target, which is exposed to a stream of low-energy (25−70 eV) ions, atoms, and electrons emerging from a low-pressure plasma discharge. Interestingly, it is possible to enrich the filled fullerenes by means of HPLC, using phases commonly employed for separations in PAH's and fullerenes.[9−11] The actual separation mechanism, however, has yet to be revealed. One of the striking features of endohedral fullerenes such as $N@C_{60}$ is their unexpectedly high thermal stability; an escape barrier of ∼1.6 eV has been reported.[6] $N@C_{60}$ molecules were successfully subjected to reactions known from ordinary C_{60}, leading to the creation of spin-probelike species.[12] Interestingly, only a single account of hydrogen(T) trapped in fullerenes ($^3H@C_{60}$) has been

† Present address: Institue of Chemistry: Metalorganics and Inorganic Materials, Technical University of Berlin, Strasse der 17. Juni 135, Sekr. C2, 10623 Berlin, Germany.

‡ Present address: Department of Natural and Behavioral Sciences, Marian College, Indianapolis, IN 46222.

(1) Prassides, K.; Dennis, T. J. S.; Christides, C.; Roduner, E.; Kroto, H. W.; Taylor, R.; Walton, D. R. M. *J. Phys. Chem.* **1992**, *96*, 10600−10602.
(2) Dilger, H.; Roduner, E.; Scheuermann, R.; Major, J.; Schefzik, M.; Stösser, R.; Päch, M.; Fleming, D. G. *Physica B (Amsterdam)* **2000**, *289*, 482−486.
(3) Liu, S. Y.; Sun, S. Q. *J. Organomet. Chem.* **2000**, *599*, 74−86.
(4) Saunders, M.; JimenezVazquez, H. A.; Cross, R. J.; Poreda, R. J. *Science* **1993**, *259*, 1428−1430.
(5) Saunders, M.; Jimenezvazquez, H. A.; Cross, R. J.; Mroczkowski, S.; Gross, M. L.; Giblin, D. E.; Poreda, R. J. *J. Am. Chem. Soc.* **1994**, *116*, 2193-2194.
(6) Waiblinger, M.; Lips, K.; Harneit, W.; Weidinger, A.; Dietel, E.; Hirsch, A. *Phys. Rev. B* **2001**, *63*, 5421.
(7) Weidinger, A.; Waiblinger, M.; Pietzak, B.; Murphy, T. A. *Appl. Phys. A: Mater. Sci. Process.* **1998**, *66*, 287−292.
(8) As described in the Experimental section, two of our samples were provided by the Hahn-Meitner Institute group; these were prepared in this way.
(9) Yamamoto, K.; Saunders, M.; Khong, A.; Cross, R. J.; Grayson, M.; Gross, M. L.; Benedetto, A. F.; Weisman, R. B. *J. Am. Chem. Soc.* **1999**, *121*, 1591−1596.
(10) Waiblinger, M. diploma work, Universität Konstanz, 1997.
(11) Goedde, B. Thesis, Darmstadt, 2001.
(12) Dietel, E.; Hirsch, A.; Pietzak, B.; Waiblinger, M.; Lips, K.; Weidinger, A.; Gruss, A.; Dinse, K. P. *J. Am. Chem. Soc.* **1999**, *121*, 1, 2432−2437.

published so far;[13] as a source of ^{3}H, the highly efficient neutron capture of ^{3}He-yielding hot recoil tritium was used.

Three stages may be discerned in the "life cycle" of H@RT_8: the filling process, the filled cage, and (the various) detrapping processes. The last stage can be brought about by different means, e.g., attack by radiolytically generated species or by nucleophiles, such as OH^-, or by thermal excitation, as discussed in this work. Additionally, we found that exposure to short-wavelength light ($\leq$ 350 nm) leads to irreversible detrapping of hydrogen and deuterium from octasilsesquioxane cages both in solid form and in solution. However, these results are not considered here.

Here, we wish to report both experimental and theoretical results concerning the energetics of the thermal detrapping of atomic hydrogen and deuterium from octasilsesquioxanes and a germaheptasilsesquioxane. Moreover, this report addresses the temperature dependence of the ^{29}Si-superhyperfine splitting constants.

Experimental Methods and Materials

All silsesquioxanes and the germasilsesquioxane were prepared according to previously published methods.[14−18] For RT_8 with R = Pr (*n*-propyl), c-Hx (cyclohexyl) samples were irradiated in a ^{60}Co-irradiator as nitrogen-purged solutions of the octasilsesquioxane (0.043 mol/L) and phenol (0.08 mol/L) in cyclopentane/cyclohexane mixtures (1:1 vol) at ~30−40 °C (internal temperature of the irradiator). The solutions were subsequently evaporated under reduced pressure. The remaining yellowish solids were quickly purified by flash chromatography using a column of silica and/or activated alumina and cyclopentane as solvent. HT_8, MeT_8, and Q_8M_8 (R = trimethylsiloxy) were irradiated as solids without any additives at the same temperature. Doses were in the range of several tens of kGy. In the case of the germasilsesquioxane, amounts of ~50−60 mg each were sealed into evacuated quartz capillaries and irradiated at 77 K. To remove radiation-induced paramagnetic defects from the quartz, one end of each ampule was annealed with a microtorch while keeping the end containing the sample submerged in liquid N_2 at 77 K, and the ampule subsequently inverted to transfer the sample into the annealed end. A sample of mixed H@MeT_8 and D@MeT_8 produced by the ion implantation process described above was kindly provided by the group of A. Weidinger, (Hahn Meitner Institute, Berlin, Germany). Solutions in toluene (A. R. grade) were purged before EPR measurement with N_2, (oxygen free, <0.5 ppm O_2) for at least 15 min. All EPR spectra were recorded on a Bruker ER100 X-band spectrometer, equipped with a TE_{102} rectangular cavity and a platform-independent data acquisition module (Model 401-012, Scientific Software Services; Normal, IL). Typical acquisition parameters at 9.89 GHz were 26 dB attenuation corresponding to 0.5 mW microwave power, sweep width 5 G or less, modulation frequency 100 kHz, modulation amplitude 0.1 G or less in solution and 1 G or less in solids. To adjust the sample temperature, a Varian CFT20 variable temperature controller was used. The sample temperature was measured using a thermocouple within the sample (Copper/Constantan lacquered, wire diameter 60 μm, homemade), connected to a digital thermometer (OMEGA, HH21), the accuracy being better than $\pm$0.3 K. The decay of the H atom signal was followed in two modes: at lower temperatures, subsequent spectra were recorded at a rate from ~1/63 s to ~1/23 s; at higher decay rates (usually for RT_8 and temperatures >110 °C), the spectrometer was operated in an on-peak mode (no field scan). For an intermediate range of temperatures, the two methods were shown to be in excellent agreement. Data evaluation (*Origin 5.0*, LabTalk, OriginLab) was performed by fitting polynomials (RT_8) or first-derivative Gaussian curves (Si_7Ge) to the EPR peaks to eliminate noise. Line shapes were not considered in detail except to ensure that lines were not broadened or otherwise skewed by saturation or modulation effects. As there was no detectable change in line widths in the course of decay, peak-to-peak amplitudes (I_{pp}) instead of double integrals served as measures of intensity.

Computational Methods

All the calculations presented here used the Gaussian 98 program,[19] with the predominant method employed being the B3LYP variant of Kohn−Sham density functional theory (DFT).[20] This is a "hybrid" technique that admixes a small amount of exact (Hartree−Fock) exchange into the exchange-correlation functional according to

$$E_{xc} = aE_x^{Slater} + (1-a)E_x^{HF} + bE_x^{Becke} + cE_c^{LYP} + (1-c)E_c^{VWN} \quad (1)$$

where the parameters *a*, *b*, and *c* are obtained empirically by "training" to the *Gaussian 1* molecule set.[21] Of particular relevance to these calculations is the parameter *a*, which is fixed at 0.8. In pure Kohn−Sham DFT, the exchange interaction is local, and the purpose of admixing a fraction (1 − *a*) of Hartree−Fock exchange in this functional is to recover some part of the nonlocality of the relationship between the exact exchange energy and the density. (The Becke exchange functional itself is nonlocal only in the limited sense that it is gradient-corrected, like the LYP term in the correlation part. Whereas the "correlation hole" is essentially local in molecular systems, the "exchange hole" is nonlocal in a sense that cannot be rectified by gradient corrections alone.) This approach is somewhat crude, and it has long been known that for some very simple systems, DFT gives seriously erroneous energy estimates: an example is the homolytic scission of H_2^+, where the fact that the exchange hole is normalized to orbital occupancy by one electron (rather than half an electron) leads to overrepresentation of exchange stabilization at large internuclear separation. The problem, in fact, applies everywhere that electron delocalization exists and is acute in a system having the possibility of spin unpairing. This has been the subject of recent concern, and improved methods (in which the degree of exact exchange admixture can be "tuned" to the extent of delocalization present) are in development,[22] but these have not to date been implemented in readily available computational packages. Consequently, we apply caution in our interpretation of results obtained from DFT and, where possible, perform supplementary calculations using conventional Hartree−Fock (ROHF, UHF) and post-Hartree−Fock (MP2) methods.

A variety of basis sets are used in this work, mostly the well-known sets of Pople and co-workers, usually supplemented with polarization functions and diffuse functions (to minimize the effects of basis set superposition error). Note that the 6-311G basis set implies the use of a McLean-Chandler basis[23] for Si and the basis set of Curtiss and co-workers[24] for Ge; this latter basis set includes explicit first-order correction due to spin−orbit coupling but neglects the small second-order SO term that affects states having spin degeneracy. The effect of this factor on the results presented here is likely to be negligible.

Results and Discussion

Experimental. In all cases studied here, the detrapping of encaged hydrogen atoms was found to follow a first-order rate

(13) JimenezVazquez, H. A.; Cross, R. J.; Saunders, M.; Poreda, R. J. *Chem. Phys. Lett.* **1994**, *229*, 111−114.
(14) Agaskar, P. A. *Inorg. Chem.* **1991**, *30*, 2707−2708.
(15) Olsson, K. *Arkiv för Kemi* **1958**, *13*, 367.
(16) Barry, A. J.; Daudt, W. H.; Domicone, J. J.; Gilkey, J. W. *J. Am. Chem. Soc.* **1955**, *77*, 4248−4252.
(17) Hoebbel, D.; Wieker, W. *Z. Anorg. Allg. Chem.* **1971**, *384*, 43−52.
(18) Feher, F. J.; Newman, D. A.; Walzer, J. F. *J. Am. Chem. Soc.* **1989**, *111*, 1741−1748.
(19) Frisch, M. J., et al. *Gaussian 98*, revision A.7; Gaussian, Inc: Pittsburgh, PA, 1998.
(20) Becke, A. D. *J. Chem. Phys.* **1993**, *98*, 5648−5652.
(21) Pople, J. A.; Head-Gordon, M.; Fox, D. J.; Raghavachari, K.; Curtiss, L. A. *J. Chem. Phys.* **1989**, *90*, 5622−5629.
(22) Becke, A. D. *J. Chem. Phys.* **2000**, *123*, 4020−4026.
(23) McLean, A. D.; Chandler, G. S. *J. Chem. Phys.* **1980**, *72*, 5639−5648.
(24) Curtiss, L. A.; McGrath, M. P.; Blaudeau, J.-P.; Davis, N. E.; Binning, J. R. C.; Radom, L. *J. Chem. Phys.* **1995**, *103*, 6104−6113.

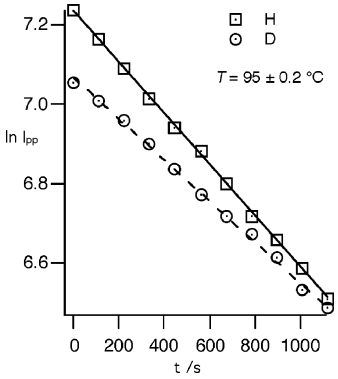

Figure 1. Logarithm of peak intensity vs time for H@MeT_8 and D@MeT_8 at 95 °C.

Table 1. Decay Rate Constants for Differently Prepared Samples of H@MeT_8

production method	T[a]	k[b]
γ-irradiation	78.1	9.601 ± 0.008
D ion implantation	78.7	9.704 ± 0.050

[a] Temperature in °C. [b] Decay rate constant in 10^{-5} s^{-1}.

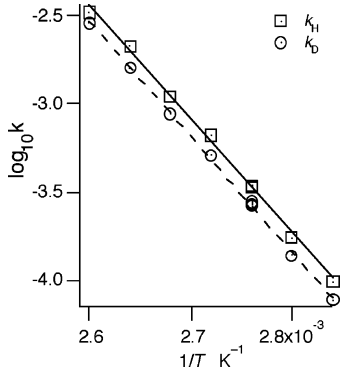

Figure 2. Arrhenius plot for detrapping of H and D from MeT_8. Rate constants k are in s^{-1}.

Table 2. Activation Parameters for Detrapping of H and D from MeT_8

sample	E_a[a]	log A[b]
H@MeT_8	126.7 ± 1.2	14.79 ± 0.17
D@MeT_8	127.4 ± 1.2	14.79 ± 0.18

[a] Activation energy in kJ mol^{-1}. [b] Frequency factor in Hz.

law as exemplified in Figure 1. Moreover, the presence or absence of oxygen had no influence on the decay rate. This holds not only for the cases of H@MeT_8 or H@HT_8, where it is known from previous studies that oxygen is not able to enter the crystal lattices,[25] but also for PrT_8 and c-HxT_8, which represent typical alkyl octasilsesquioxanes. Because of the way the filled octasilsesquioxanes were produced, we were concerned about (a) the influence of reactive radical species, which are present, e.g., in irradiated MeT_8 and HT_8, and (b) the influence of peroxides, which are formed due to the fact that the irradiation occurs in the presence of molecular oxygen (Q_8M_8). To address (a), we compared the decay of a γ-irradiated sample to the decay of a sample that was produced by the ion implantation approach using deuterium projectiles. The latter sample did not show any signal due to $O_{3/2}Si-CH_2^{\bullet}$ entities, whereas this signal is dominant in the spectrum of γ-irradiated MeT_8. As Table 1 shows, the rate constants determined for the two methods differ by less than a percent. This result indicates that species such as $O_{3/2}Si-CH_2^{\bullet}$, despite their high concentration in the irradiated solids, do not interfere with the detrapping process but undergo independent decay reactions within the lattice instead.

The previously mentioned technique of ion implantation allowed the preparation of D@MeT_8, which was not possible by the deuterated solvent approach because of the extremely low solubility of MeT_8. As mentioned above, using D_2 as plasma gas did not result in solely D-filled cages but, in fact, yielded a mixture, of which about 48% (from the areas of the EPR-signals) of the filled cages carried an H atom and just 52% carried a D atom. To account for this result, it should be kept in mind that even though low-energy ions (20−70 eV) were used, their energy is "unchemically" high and, thus, quite severely damaged samples are produced. This holds equally for the fullerenes[6] and may be illustrated by the fact that after the ion implantation treatment, a large portion of C_{60} (N_2^+ ions) and about 75% of an EtT_8 sample (D_2 as plasma gas) are found insoluble. Evidently, the process of filling takes place at least in part in the sublimate, where the density of potential traps is much higher than in the gas phase. The previous statement is also supported by the fact that even with nitrogen projectiles, a yield of H@MeT_8 was obtained.

For our purposes, the presence of both H@MeT_8 and D@MeT_8 in the same sample proved advantageous insofar as the detrapping of H and D could be followed in a single sample at exactly the same temperature. This fact and the improved experimental setup enabled us not only to obtain more precise activation parameters for a few octasilsesquioxanes but also to detect a kinetic isotope effect for the detrapping of H and D. At all temperatures, the signal due to H@MeT_8 decayed faster than the corresponding D signal. This is shown in Figure 1 for the temperature of 362.8 K. Figure 2 shows an Arrhenius plot, summarizing the decay rates at seven different temperatures in the range of 280.3−380 K, whereas Table 2 gives the extracted activation parameters.

For experimental reasons, it is harder to follow the reaction at temperatures outside this range. For slower decay rates, the stability of the spectrometer starts to matter, and for higher rates, the heat transfer within the sample to reach a homogeneous temperature profile is slow compared to the reaction. The extracted ΔE_a of 0.73 kJ mol^{-1}, although smaller than the margin of error, is consistent with the difference between the zero-point energies of H and D in the potential wells of the cages. This will be shown in the section concerning theoretical results. Similar observations have recently been reported by Hayashino et al.[26]

A somewhat different approach had to be taken to study the detrapping of H from germaheptasilsesquioxane, hereafter denoted Si_7Ge. First attempts to trap H inside these cages by simply irradiating samples of Si_7Ge under the same conditions used for RT_8 (at or above room temperature, access of air) proved unsuccessful. Therefore, samples of Si_7Ge were sealed in evacuated EPR tubes and irradiated at 77 K (Dose 80 kGy). The irradiated samples were stored at the same temperature and measured within 24 h of irradiation.

(25) Päch, M.; Stösser, R. *J. Phys. Chem. A* **1997**, *101*, 8360−8365.

(26) Hayashino, Y.; Isobe, T.; Matsuda, Y. *ChemPhysChem* **2001**, 748−750.

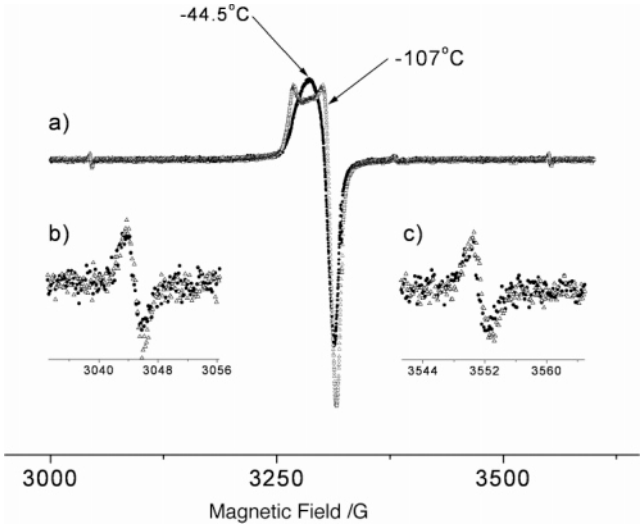

Figure 3. EPR spectrum of solid irradiated Si_7Ge. (a) Survey spectrum, (b) low field, and (c) high field signals from H trapped in methylgermaheptasilsesquioxane cage. Central line with indicated temperature dependence is from peroxyl radicals.

A typical spectrum of these samples is shown in Figure 3. The major, central part of the spectrum is due to peroxyl radicals, resulting from the reaction of C-centered radicals with residual traces of O_2 during the irradiation. They show a typical temperature dependence due to rotational movement.[27] The smaller signals at ~3040 and ~3550 G prove the successful stabilization of H in the sample. It seems reasonable to attribute the low intensity of these signals to unfavorable lack of scavengers[25] in the evacuated tubes. Nevertheless, even under these circumstances, it was possible to follow the decay, but only within a temperature range from 288 to 316 K. Because of the noisier data (see Figure 3b,c), we did not use the polynomial fitting function for evaluation but the more restrictive first derivative of a Gaussian function.

An example of the results of these measurements is shown in Figure 4a, and the corresponding Arrhenius plot is shown in Figure 4b. Despite the comparatively large margins of error, which are due to the quite limited range of temperatures and the noisy data, it is obvious that this system is characterized by both a lower activation energy (115.2 ± 4.1 kJ mol^{-1}) and a higher preexponential factor (log *A*: 16.57 ±0.71). Table 3 collects these data in comparison to those for H and D in other RT_8 systems. While this manuscript was in preparation, brief reports[26,28] of similar trapping and ESR detection experiments have appeared.

The temperature dependence of hyperfine parameters often provides useful insights into the dynamics of paramagnetic systems. The proton and deuteron couplings of trapped hydrogen isotopes were studied as a function of temperature by Dilger et al., who additionally obtained one data point (at room temperature) for the light hydrogen isotope muonium.[2] To extend the available data to other nuclei, we studied the temperature dependence of the ^{29}Si-shf coupling constant using a mixed sample of H@PrT_8 and D@ PrT_8. A typical partial spectrum is shown in Figure 5a. The peaks marked by an arrow are almost exclusively due to {H,D}@$^{29}Si^{28,30}Si_7$, which account for about

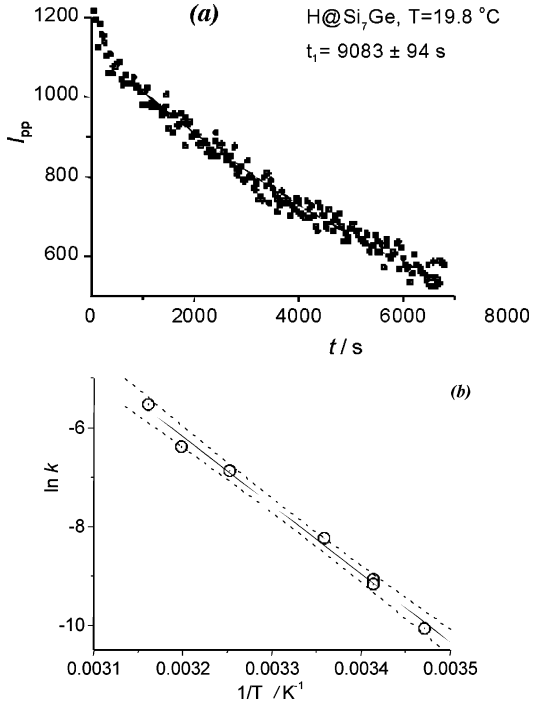

Figure 4. (a) Thermal decay of H@Si_7Ge. (b) Arrhenius plot for the decay over the range 15−43 °C. Dashed line 95% confidence level (level used throughout); errors in individual data points are less than the symbol size.

Table 3. Observed Activation Parameters for Atomic Hydrogen (and Deuterium) in Different Cages

system	E_a[a]	log A[b]
HT_8	126.4 ± 1.9	14.82 ± 0.27
H@MeT_8	125.0 ± 1.4	14.54 ± 0.20
D@MeT_8	126.4 ± 0.8	14.66 ± 0.12
PrT_8	123.3 ± 0.7	14.41 ± 0.09
c-HxT_8	122.8 ± 1.1	14.36 ± 0.15
Q_8M_8	122.7 ± 1.4	14.14 ± 0.19
Si_7Ge	115.2 ± 4.1	16.57 ± 0.71

[a] Activation energy for trapping in kJ mol^{-1}. [b] Frequency factor in Hz.

26.8% of all isotopomers present. Contributions due to cages with ≥3 ^{29}Si atoms are negligible (altogether less than 0.482%), whereas cages having two ^{29}Si nuclei have an abundance of about 4.9%. The sample was dissolved in toluene in an EPR tube equipped with an internal thermocouple and purged with N_2. Figure 5b shows that for both the H- and the D-filled cages, the coupling constant exhibits a negative temperature coefficient, which, however, differs for H and D. A qualitative explanation for this behavior is given in the Conclusions section.

Computational. Basic structure-energy calculations on H trapping in, and escape from, the simplest octasilsesquioxane cage, HT_8, have been published by Mattori et al.,[29] who optimized the structure with and without H at the cage center and performed a further calculation on the face-centered H-escape transition state (TS). The optimization was carried out at the B3LYP/6-31G** level for the empty cages (a larger 3s2p1d basis was used on the trapped hydrogen in the filled cages) and within the point groups O_h (HT_8, H@HT_8) and C_{4v} (H−HT_8 TS). Additional spin density calculations were carried out at the UHF, B3LYP, and MP2 levels using the above mixed basis set and a second basis set in which the trapped atom basis

(27) Rhodes, C. J. In *Peroxyl Radicals*; Alfassi, Z., Ed.; J. Wiley & Sons: New York, 1997; p 335.
(28) Hayashino, Y.; Isobe, T.; Matsuda, Y. *Inorg. Chem.* **2001**, *40*, 2218-+.
(29) Mattori, M.; Mogi, K.; Sakai, Y.; Isobe, T. *J. Phys. Chem. A* **2000**, *104*, 10868−10872.

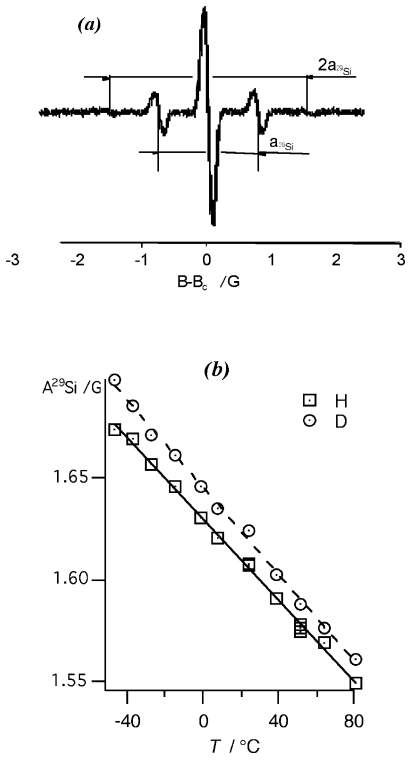

Figure 5. (a) Partial EPR spectrum for H@PrT_8 in deoxygenated toluene showing ^{29}Si superhyperfine coupling. (b) Temperature dependence of the ^{29}Si coupling constant for H and D@PrT_8 in toluene. Linear fits are $a_D(^{29}\text{Si}) = 1.6454 \pm 0.0008\ G - (0.00107 \pm 0.00002)G/K \times T$ and $a_H(^{29}\text{Si}) = 1.6296 \pm 0.0006\ G - (0.00100 \pm 0.00013)\ G/K \times T$.

set was further augmented with compact *s*-functions. They obtain detrapping barriers and encapsulation energetics (H is always more stable *outside* the cage) as follows: $\Delta E_d \equiv E_{TS} - E_{H@RT_8} = 128.7$ kJ mol^{-1} (MP2), 98.6 kJ mol^{-1} (B3LYP); $\Delta E_{stab} \equiv E_{H+RT_8} - E_{H@RT_8} = -9.3$ kJ mol^{-1} (MP2), -26.1 kJ mol^{-1} (B3LYP). They note that their B3LYP calculations are in the closest agreement with the experimental data of Päch et al.;[25] however, the present experimental results, which represent an improvement on that work, lie closer to their MP2 values. More recently Kaupp et al., in a study focused primarily on g-tensor properties, carried out calculations on several H@RT_8 species using DFT-based methods,[31] and a limited set of B3LYP/6-31G calculations were undertaken on H@HT_8 by Dinse.[32] All these calculations will be considered in the context of our own work in the following.

The structures of the bare cage and the H-centered cage have O_h symmetry and are completely described by the three parameters, r_{Si-O}, r_{Si-H}, and $\vartheta_{Si-O-Si}$ ($\equiv\vartheta$). An origin-centered set of Cartesian coordinates is then given by

$$\boldsymbol{r}(\text{Si}) = (\pm r_1, \pm r_1, \pm r_1) \tag{2}$$

where

$$r_1 = r_{\text{Si-O}} \sin\left(\frac{\vartheta}{2}\right) \tag{3}$$

$$\boldsymbol{r}(\text{O}) = (0, \pm r_2, \pm r_2) \tag{4}$$

and variations thereof with zero in the *y* and *z* positions, where

$$r_2 = r_{\text{Si-O}}\left(\sin\left(\frac{\vartheta}{2}\right) + \frac{1}{\sqrt{2}}\cos\left(\frac{\vartheta}{2}\right)\right) \tag{5}$$

and

$$\boldsymbol{r}(\text{H}) = (\pm r_3, \pm r_3, \pm r_3) \tag{6}$$

where

$$r_3 = r_1 + \frac{r_{\text{Si-H}}}{\sqrt{3}} \tag{7}$$

If the cage is terminated with methyl groups rather than H atoms, the carbon positions are given by

$$\boldsymbol{r}(\text{C}) \equiv r_{3a} = r_1 + \frac{r_{\text{Si-H}}}{\sqrt{3}} \tag{8}$$

whereas the H-atom positions depend on the methyl-group orientations. Distinguishing eclipsed (methyl C−H bond eclipses Si−O bond) and staggered (methyl C−H bond lies equidistant between two Si−O bonds) limiting geometries, and using two further structural parameters, r_{C-H} and γ_{Si-C-H} ($\equiv\gamma$), we define two further pairs of new terms

$$r_4^{\pm} = \frac{r_{\text{C-H}}}{\sqrt{6}}(\sqrt{2}\cos\gamma \pm \sin\gamma) \tag{9a}$$

$$r_5^{\pm} = \frac{r_{\text{C-H}}}{\sqrt{6}}(-\cos\gamma \pm \sqrt{2}\sin\gamma) \tag{9b}$$

Then, in the eclipsed geometry, the vector connecting C and H_1, the eclipsing atom, is

$$\mathbf{r}_{\text{C-H}_1} \equiv (\partial_1,\partial_2,\partial_3) = (r_4^{+}, r_4^{+}, r_5^{-}) \tag{10a}$$

and the displacement vectors of the other two H atoms (generated by $2\pi/3$ rotations around Si−C) are permutations of the elements of $\mathbf{r}_{C-H_1}$ having the form

$$\mathbf{r}_{\text{C-H}_2} \equiv (\partial_3,\partial_1,\partial_2) \tag{10b}$$

$$\mathbf{r}_{\text{C-H}_2} \equiv (\partial_2,\partial_3,\partial_1,) \tag{10c}$$

In the staggered geometry, the C−H_1 bond vector takes the form

$$\mathbf{r}_{\text{C-H}_1} = (r_4^{-}, r_4^{-}, r_5^{+}) \tag{11}$$

but the permutation relations for the C−H_2 and C−H_3 bond vectors still hold.

All-Si Cages. Geometrical parameters for HT_8 obtained using a variety of techniques and basis sets are summarized in Table 4. None of these calculations is methodologically identical with the work of Mattori et al. or the work of Kaupp et al. (Dinse does not publish his structural parameters), but the B3LYP results show very little dependence upon basis set (except that the smallest basis studied here, 3-21G, gave a Si−O bond that is strikingly too long), and the agreement of all these geometries

(30) auf der Heyde, T. P. E.; Bürgi, H.-B.; Bürgy, H.; Törnroos, K. W. *Chimia* **1991**, *45*, 38−40.
(31) Kaupp, M.; Asher, J.; Arbuznikov, A.; Patrakov, A *Phys. Chem. Chem. Phys.* **2002**, 4, 5458.
(32) Dinse, K.-P. *Phys. Chem. Chem. Phys.* **2002**, 4, 5442.

Table 4. Geometrical Parameters for Empty HT_8

method	r_{Si-O}[a]	r_{Si-H}[a]	ϑ[b]
HF/3-21G	1.644	1.454	152.9
HF/3-21G*	1.625	1.451	152.2
HF/6-31+G*	1.626	1.453	149.4
B3LYP/3-21G	1.666	1.468	150.7
B3LYP/3-21G*	1.639	1.464	150.4
B3LYP/6-31G*	1.643	1.465	148.1
B3LYP/6-311G**	1.642	1.461	149.4
B3LYP/6-31+G*	1.645	1.464	148.4
BPW91/6-31+G*	1.657	1.468	147.3

[a] Bond lengths in Å. [b] Si−O−Si bond angle in degrees.

with those of Mattori et al. is close. The Hartree−Fock results (again, except for those with the smallest basis) are also apparently fairly well converged. The higher-quality Hartree−Fock values lie somewhat closer to experiment[30,33] (the experimental length is 1.6195 Å), whereas both HF and B3LYP overestimate ϑ, with B3LYP coming a little closer (the experimental value is 147.5°). The bond length deviations seen in B3LYP may reflect the fact that the basis sets used here were, in fact, optimized using Hartree−Fock-based methods. Additionally, the test molecules on which these basis sets were optimized were rather small, and some error is to be expected in progressing to the larger systems treated here. A single geometry optimization was performed using the "pure" density functional method BPW91, which uses an exchange functional due to Becke[34] and one of the correlation functionals created by Perdew and Wang,[35] and the 6-31+G* basis set—this combination yielded, as might be expected, results that are different from the Hartree−Fock results by a somewhat larger amount than B3LYP, in the same direction (lengthening of r_{Si-O}, contraction of ϑ). This is consistent with the claim of Kaupp et al. that DFT tends to overestimate the length of bonds to Si;[31] the hybrid method, not unexpectedly, yields intermediate results.

Substitution of the terminating hydrogen atoms by methyl groups makes relatively little difference to the cage geometry. Calculations at the B3LYP/3-21+G* level within the point group O_h led to a parameter set (r_{Si-O}, r_{Si-C}, r_{C-H}, ϑ, γ) = (1.652, 1.856, 1.098, 152.4, 110.8), essentially the same for both the eclipsed and staggered geometries. The eclipsed geometry is in fact a local maximum along all of the methyl torsional coordinates; the staggered geometry is more stable by 23.9 kJ mol^{-1}, implying that each methyl group experiences a torsional barrier on the order of 3 kJ mol^{-1}. (The groups are sufficiently well separated that inter-group interactions are likely to be small.) Hartree−Fock calculations with the same basis set led to structural parameter sets (r_{Si-O}, r_{Si-C}, r_{C-H}, ϑ, γ) = (1.635, 1.851, 1.088, 153.7, 111.1) for the eclipsed isomer and (r_{Si-O}, r_{Si-C}, r_{C-H}, ϑ, γ) = (1.635, 1.844, 1.088, 153.4, 111.0) for the staggered isomer, with the only significant difference between the two being a slight lengthening of the Si−C bond in the eclipsed case, which is not seen in the B3LYP calculations. At the Hartree−Fock level, the energy separation between isomers is 27.9 kJ mol^{-1}.

Other Homonuclear Cages. That the stability of octahedral sesquisiloxane cages is a consequence of the flexibility in valence angles characteristic of the second row of the periodic table seems clear from the fact that for a cage in which all silicon atoms have been replaced with carbon atoms, the O_h structure now yields a single imaginary vibrational frequency corresponding to a mode with A_2 symmetry ($\nu \approx 155i$ cm^{-1} at the B3LYP/6-31+G* level) whereas the global energy minimum (though still cubic from the perspective of the corner atom positions) at the B3LYP/6-31+G* level now has the rather uncommon T_h symmetry and the structure shown in Figure 6a. (The body diagonals are C_3 axes, but do not contain symmetry planes.)

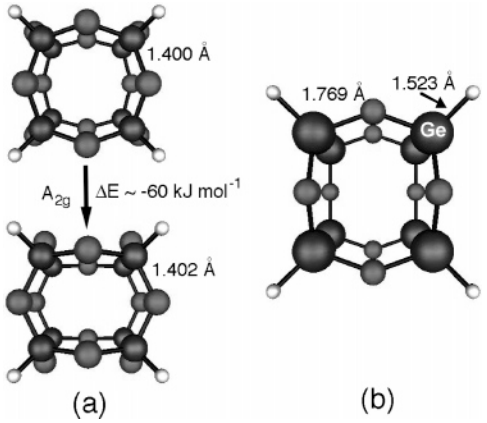

Figure 6. Optimized geometries for (a) $C_8O_{12}H_8$ and (b) $Ge_8O_{12}H_8$.

The degree of distortion from O_h can, in this case, be characterized by a parameter expressing the displacement of the oxygen atoms from their high-symmetry positions. Where in O_h the oxygen atoms had coordinates of the type (0, r_2, r_2), in the T_h system, two parameters, r_2 and r_2', must be defined, and each oxygen atom has coordinates which are some permutation of (0, r_2, r_2'). A suitable normalized distortion parameter might then be

$$\tau \equiv \frac{|r_2 - r_2'|}{r_2 + r_2'} \tag{12}$$

For the C_8 cage at this level of computation $\tau \approx 0.16$, and the lowest-frequency modes are at 221 cm^{-1} (T_u) and 222 cm^{-1} (A_g), showing that this is unambiguously a minimum.

A similar cage in which all the corner atoms are germanium, however, is computationally more ambiguous, with results showing a dependence on method, basis set, choice of pure versus Cartesian d-functions, and choice of default versus unpruned spherical-product integration grids. The valence-only LANL2DZ basis set (where the heavy-atom inner electrons are replaced by pseudopotentials) led to an octahedral structure both with RHF and B3LYP, whereas all-electron basis sets led to values of τ varying from 0.082 (RHF/6-311G*) to 0.195 (B3LYP/3-21G*) for basis sets not including diffuse functions. (The inclusion of diffuse functions for this system leads to problems ranging from convergence difficulties (B3LYP/6-31+G*) to strong dependence on the type of d-functions used, suggesting that linear near-dependency or similar problems may be present.) The representative distorted structure shown in Figure 6b was obtained at the B3LYP/6-311G* level (where the basis set is optimized for, and uses, pure d-functions), and has $\tau = 0.131$. In the octahedral systems, the angle at oxygen (which we have defined above as ϑ) is 133.7° in the carbon cage and (approximately) 151° in the germanium cage, whereas

(33) Törnroos, K. W. *Acta Crystallogr., Sect. C: Cryst. Struct. Commun.* **1994**, *50*, 1646−1648.
(34) Becke, A. D. *Phys. Rev. A: At., Mol., Opt. Phys.* **1988**, *38*, 3098−3100.
(35) Perdew, J. P.; Wang, Y. *Phys. Rev. B: Condens. Matter Mater. Phys.* **1992**, *45*, 13244.

Table 5. Geometrical Parameters for H@HT_8

method	r_{Si-O}[a]	r_{Si-H}[a]	ϑ[b]
B3LYP/6-31G*	1.642	1.463	150.0
B3LYP/6-311G**	1.645	1.461	150.0
BPW91/6-31+G*	1.659	1.475	146.7
UHF/6-31+G*	1.629	1.453	149.2

[a] Bond lengths in Å. [b] Si−O−Si bond angle in degrees.

the inner angles at the corner atoms are 115.7° and ∼109°, respectively. In the T_h carbon cage, the angles are 128.9° at O and 114.5° at the vertexes, indicating a small degree of strain relief at C and O due to the distortion.

H Trapping and Desorption. As described by Mattori et al.[29] for HT_8, the trapping of a hydrogen atom in these cages leads to a small degree of cage swelling and a potential minimum in which the trapped atom lies at the cage center. The overall system (in the case of H@HT_8) retains its O_h symmetry. The converged structural parameter values for H@HT_8 obtained using several different technique/basis set combinations are summarized in Table 5. The B3LYP numbers are broadly in agreement with the results of Mattori. Again, Hartree−Fock calculations (unrestricted, in this case) lead to Si−O bond lengths shorter than those obtained in the density functional methods.

The structural changes in MeT_8 on H encapsulation are similar, with UB3LYP/3-21+G* yielding values of (r_{Si-O}, r_{Si-C}, r_{C-H}, ϑ, γ) = (1.655, 1.849, 1.098, 151.8, 110.7), the slight swelling of the cage to accommodate the H atom being exemplified by both the small increase in r_{Si-O} and the opening out of the Si−O−Si angle. The only other change of interest from the HT_8 system is that here the Si−C bonds shorten noticeably on cage filling.

The H (de)trapping transition state geometries were studied for both HT_8 and MeT_8, in both cases using C_{4v} symmetry. In the case of HT_8, the Si−O bond in the face through which the H atom is passing (known hereafter as the "front" face) is stretched to accommodate its passage, taking values of 1.676 Å in UB3LYP/3-21+G* and 1.671 Å in UB3LYP/6-31+G*. The Si−O−Si bond angle, however, *narrows* to 143.8° (3-21+G*) (141.7° in 6-31+G*), indicating that this effect is due predominantly to an outward displacement of the O atoms. This feature is consistent with the observation that the barrier maximum is associated with traversal of the plane defined by the oxygen atoms (and the relevant coordinate shows an inward−outward counter movement of H and O at the transition state). The rear face of the cage has Si−O bonds essentially identical in length to those of the empty cage, but exhibits Si−O−Si angles intermediate between those in the empty/filled cage and those in the front face, at 147.9° in 3-21+G* and 145.2° in 6-31+G*. By contrast, the side faces show Si−O−Si bonds that have opened out substantially, to 160.1° in 3-21+G* and 155.0° in 6-31+G*. The essence of the distortion is confirmed by consideration of the Si−Si face diagonal, which is actually *contracted* in both the front and rear faces with respect to its values, even in the unfilled cage. For example, in B3LYP/6-31+G*, the face diagonal shrinks from 4.478 Å in the empty cage to 4.466 Å in the front face of the transition state geometry and 4.444 Å in the rear face. The outward displacement of the oxygen four-ring was noted by Mattori et al.,[29] though the full character of the transition state geometry was not discussed.

Table 6. Calculated Trapping/Detrapping Energetics[a] for H in HT_8 and MeT_8

system	basis	E_a[b]	$E_{a'}$[c]	ΔE[d]
H + HT_8	3-21G*	126.4	95.4	31.0
	3-21G*[e]	181.8	126.4	55.3
	3-21+G*	138.8	107.5	31.3
	6-31+G*	135.7	102.6	33.1
H + MeT_8	3-21+G*	138.1	106.3	31.9
	6-31+G*	138.7	101.2	37.5

[a] Calculated from the B3LYP model. [b] Activation energy for trapping in kJ mol^{-1}. [c] Activation energy for detrapping in kJ mol^{-1}. [d] Energy difference. [e] Unrelaxed geometry (see text).

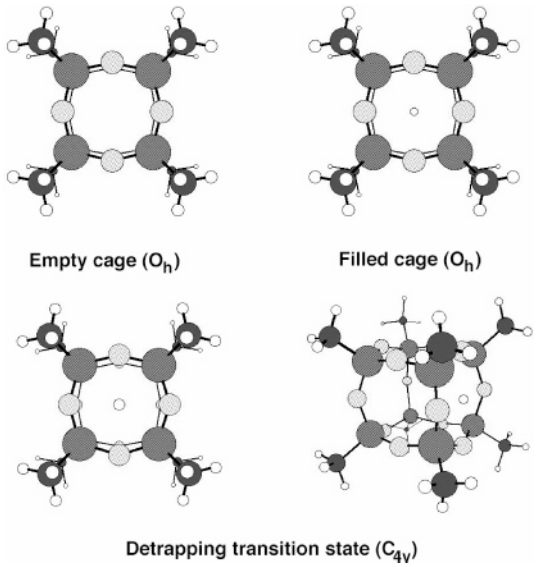

Figure 7. Optimized geometries of MeT_8 and H@MeT_8 and two views of the detrapping transition state.

Similarly, in MeT_8, the transition state geometry has Si−O bond lengths of 1.678 Å in the front face, accompanied by Si−O−Si angles of 145.6°. Meanwhile, the Si−O−Si angle in the side face has opened up to 157.9°. The Si−Si face diagonals of 4.535 and 4.509 Å in the front and rear faces compare to 4.535 Å in the empty cage and 4.551 Å in the filled cage.

The energetics of (de)trapping in the H+HT_8 and H+MeT_8 systems were calculated using the B3LYP method, employing several small basis sets and, in the case of HT_8, studying the effect of relaxation on the energies by obtaining the equivalent parameters based on a nonrelaxing cage (at the HF/3-21G* optimized geometry). The resultant energy parameters E_a (the trapping barrier), $E_{a'}$ (the detrapping barrier), and $\Delta E_@$ (the energy increase of the overall system on encapsulation with respect to isolated H and RT_8) are collected in Table 6. The relevant geometries of MeT_8, H@MeT_8, and the detrapping transition state are shown in Figure 7.

Aspects of the Trapping Potential. The values obtained from fully relaxed calculations on H + HT_8 are similar to those published by Mattori et al.;[29] the small differences are attributable to differences in the basis set used. Strikingly, there is almost no difference between results on H + HT_8 and H + MeT_8 at the same level. Because the terminating groups seem to make very little difference to the trapping potential (at least in the case of H atoms vs alkyl groups), we use the minimal HT_8 system for the majority of our more detailed calculations.

We note, however, that our present experimental data, which are of higher quality than the previously published data, are in

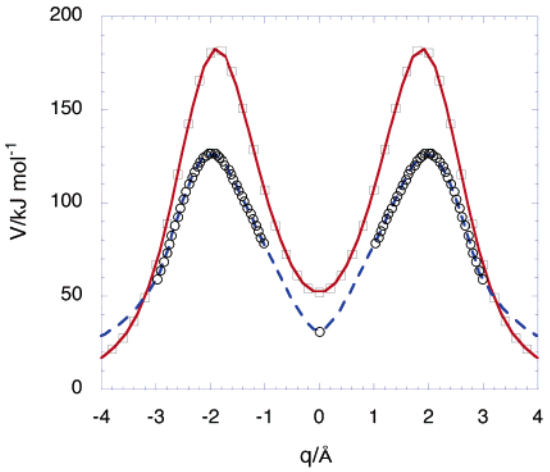

Figure 8. Comparison of rigid and relaxed detrapping potentials in H@HT_8 (B3LYP/3-21G*).

better agreement with Hartree−Fock or MP2[29] results (i.e., higher barrier) than with the density functional results (i.e., lower barrier). This may originate in a weakness of the DFT description of the electronic structure (both the encapsulated O_h structure and the post-escape C_{4v} structure have relatively weak H-cage interactions, whereas the interaction is at its strongest when the H atom is passing through the plane defined by four facial O atoms; at this point, any delocalized exchange effects, which have a stabilizing influence, will be at their most severe) or may be due to incomplete adiabaticity of the escape process. (Though there is no experimental evidence for a tunneling contribution to the escape process, it may be that the thermally excited caged atom is vibrationally sufficiently decoupled from the motions of the cage itself to yield a higher net escape barrier.)

One-dimensional potentials (along the face center−face center axis) were calculated for H detrapping from HT_8 at several levels of theory and both with and without allowing the relaxation of the other geometrical parameters. The off-center geometries were constrained to C_{4v} symmetry through appropriate coordinate definitions. The total energy as a function of the full exit path coordinate (calculated by computing the intrinsic reaction coordinate downhill from the exit saddle point in both directions) is shown in Figure 8, which gives a comparative view of the rigid and relaxed potentials.

It is clear that the deviation between the potentials occurs mainly in the close vicinity of the barrier-crossing geometry and, therefore, that the potential for motions near the cage center can be calculated with reasonable accuracy within the rigid-cage approximation. By the same token, the zeroth-order assumption of independence of the motions of the cage and the encapsulated H atom (implicit, e.g., in the treatment of the isotopic variation of the hyperfine coupling and its temperature-dependence by Dilger et al.[2]) is reasonable for low-energy vibrations.

Rigid potentials and corresponding ^{1}H couplings for the encapsulated H atom calculated using several methods are presented in Figure 9a,b. To emphasize the difference between the techniques in terms of their treatment of H-cage *interactions*, the potentials are calculated relative to the asymptotic energy of the separated H + HT_8 system, determined either by fitting the tail of the potential to an exponential function or simply as the sum of the isolated subsystem energies uncorrected for

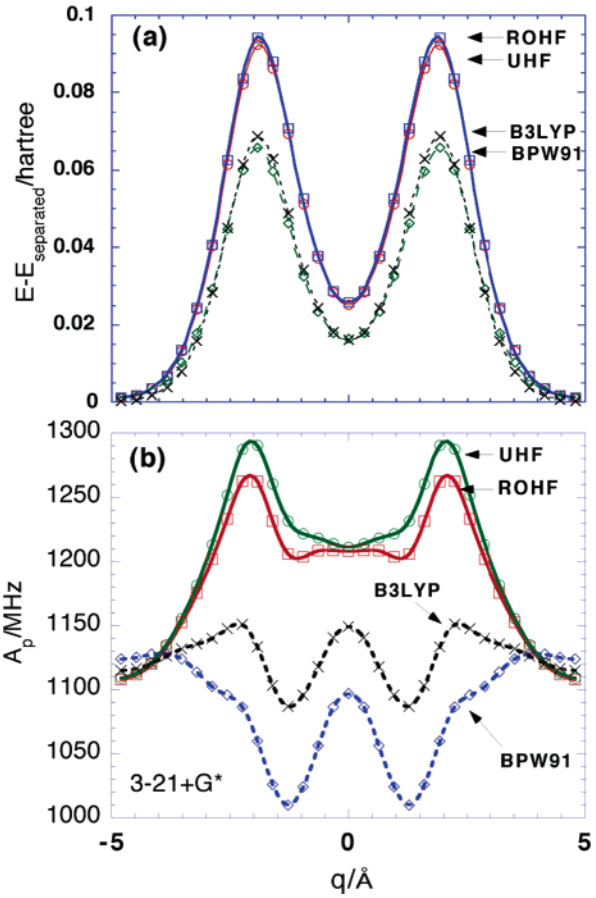

Figure 9. (a) Rigid potentials and (b) ^{1}H isotropic hyperfine coupling for H in HT_8.

BSSE. Not surprisingly, the two Hartree−Fock methods are in excellent agreement at the cage center (the very small difference visible in the figure is, in fact, a result of small disparities in the tail fitting), and even at the energy maximum, the deviation remains fairly small, on the order of 5 kJ mol^{-1}, with ROHF exhibiting the slightly larger barrier; similar observations hold for the DFT-based methods, with the energy difference at the maximum amounting this time to about 8 kJ mol^{-1}. (Either of the open-shell HF-based methods is exact for isolated H at the Hartree−Fock limit, whereas in the limit of no interaction, the cage is closed-shell, so the calculations can be expected to give asymptotically identical results. The $\langle S^2 \rangle$ values in the UHF calculations are 0.7500 for the asymptotic geometry, 0.7508 for the body-centered geometry, and 0.7534 for the barrier geometry.) More striking, though, is the difference between the energies for the O_h body-centered geometry using the two pairs of methods; the DFT-based methods give energies more stable by about 24 kJ mol^{-1} than the Hartree−Fock-based methods. The origin of this extra stability is at the moment unknown, though it could be related to delocalized exchange effects or to numerical cutoff errors in calculating the long-range interactions active here. This observation is, however, consistent with the fact that the BPW91 method yields the more stable energy *maximum* by 8 kJ mol^{-1}, whereas the difference between the UHF and the B3LYP methods is about 64 kJ mol^{-1}; the B3LYP method incorporates 20% Hartree−Fock exchange energy, of a comparable order to the fractional energy difference neglecting the extra stabilization present in the body-centered geometry.

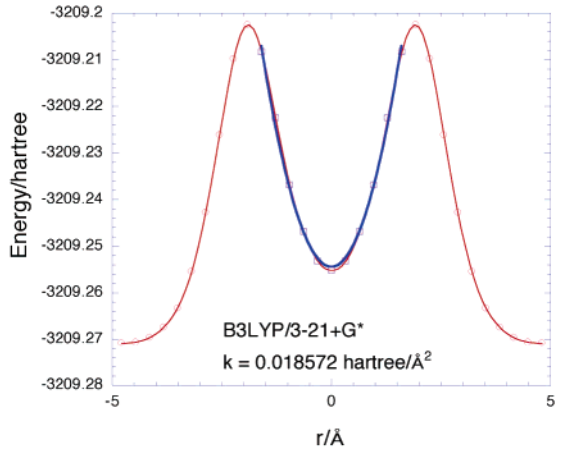

Figure 10. One-dimensional harmonic fit to the rigid intra-cage potential.

Table 7. Harmonic Parameters from Rigid-cage Potentials[a]

method	k[b]	E_0^{Hc}	E_0^{Dc}	E_0^{Muc}
B3LYP	16.2	9.37	6.63	27.9
BPW91	15.1	9.06	6.41	27.1
ROHF	21.5	10.8	7.59	32.2
UHF	21.5	10.7	7.55	31.9

[a] Cages at the BPW91/3-21+G* geometry, rigid potentials shown in Figure 13. [b] Force constant in N m^{-1}. [c] Zero-point energy for superscripted atom in kJ mol^{-1}.

Fitting the region $-r_1 < q < r_1$ (i.e., the interior of the Si cage) to a harmonic potential leads to somewhat more accurate estimates for force constants and isotope-dependent zero-point energies than can be obtained from the analytic (second-order Hellmann−Feynman) frequencies calculated at the body-centered energy minimum geometry. A sample fit (for the B3LYP method) is shown in Figure 10, and fitting results for the foregoing rigid cage data are shown in Table 7.

The differences in zero-point energy obtained from these results are in good agreement with the isotope differences in detrapping activation energy obtained from the present experimental data. The rigid model represents the fully decoupled limit between atom displacement and cage vibrations. With the assumption that the transverse mode frequencies at the transition state are the same as those at the cage center (in reality, they will be larger), the one-dimensional component of the zero-point energy difference in the longitudinal direction (i.e., one-third of the total difference) represents an upper limit for the difference in barrier height. Using the B3LYP data, for example, this leads to a value of 0.91 kJ mol^{-1}. The other methods yield comparable results. The harmonic force constants k are somewhat larger than those obtained by Roduner's group in fits to their experimental data, though it should be noted that (for EtT8 and Q8M8) they obtain a spread of k values depending on whether only H isotope data, only D isotope data, or both H and D isotope data are analyzed, implying that the value of k is quite sensitive to measurement error or weaknesses of the model.[36]

The calculated ZPE values are, accordingly, larger than those derived by Roduner's group. The value for E_0^H given by Kaupp et al., 3.0 kJ mol^{-1},[31] is smaller than that obtained by Roduner but is difficult to reconcile with their published data for energy vs H atom displacement, calculated at the UBP86/DZVP level. Fitting to the values for displacement along the cage center to face center axis published in their Table 2 leads to a value of $k = 18.2$ N m^{-1}, corresponding to $E_0^H = 9.9$ kJ mol^{-1} and in extremely good agreement with our values. On the other hand, Dinse considers displacement from the cage center in a geometrically relaxed H@HT$_8$ system at the B3LYP/6-31G level and obtains $k = 11$ N m^{-1}.[32] This leads to a harmonic eigenfrequency of 314 cm^{-1} for deuterium, in fairly good agreement with the value of 368 cm^{-1} obtained from a fit to his experimental data. This experimentally fitted value corresponds to $k = 16$ N m^{-1}, in better agreement with the present calculations (and Kaupp's) than with Dinse's. (It may be relevant here that Dinse's calculated energies, shown in Figure 6 of his paper, contain a seemingly spurious minimum at nonzero displacement from the cage center, which may have affected his fit.)

Hyperfine Couplings. The experimental vacuum value of A_p is 1420.4057 MHz,[37] whereas the low-temperature experimental encaged value (rather temperature-independent below about 100 K) is 1418.2 MHz for the Q$_8$M$_8$ cage (which has (O)SiMe$_3$ corner groups).[2] This difference may be supposed to represent a balance between wave function "compression" due to the surrounding field of negative charge and spin delocalization from the trapped atom to the cage framework. The influence of boundary conditions, electric fields, and field gradients on the energies and wave function of the hydrogen atom have been explored by several authors.[38,39] These quantities acquire a temperature dependence through the vibrational excitation of the H atom in the cage and exhibit an isotopic dependence even at low temperatures due to zero-point effects.[2] Though the Hartree−Fock method is exact for the H atom (and so systematic basis set augmentation can be expected to lead asymptotically to the exact values for the total energy and the Fermi contact interaction), the same is not true for the most widely used density functional methods; although there are exchange functionals in the literature which treat the hydrogen atom correctly, [40] the majority are exact only for the uniform electron gas.[22] Additionally, there are, in principle, numerical problems involved in calculation of the Fermi contact interaction related to the fact that typically in nonrelativistic calculations this quantity is evaluated from the spin density at the nucleus, which is dependent both on the accuracy with which the true cusp behavior can be approximated with a linear combination of Gaussian functions and on the features of the grid used in calculating integrals. Hyperfine couplings for H at the body-centered position in H@HT$_8$ were obtained (at the UB3LYP/3-21G* optimum geometry) using the UHF, B3LYP, and BPW91 techniques and a variety of basis sets—in particular, calculations with the correlation-consistent n-tuple ζ basis sets of Dunning[41−45] (modified by Davidson[46]) afford a homologous series of increasing size; for H, the cc-pvdz and cc-pvtz sets

(36) Groβ, B.; Dilger, H.; Scheuermann, R.; Päch, M.; Roduner, E. *J. Phys. Chem. A* **2001**, *105*, 10012−10017.
(37) Karshenboim, S. G. Simple atoms, quantum electrodynamics, and fundamental constants. In *Precision Physics of Simple Atomic Systems*; Lecture Notes in Physics, Vol. 627; Karshenboim, S. G., Smirnov, V. B., Eds.; Springer: Berlin, 2003; pp 141−162.
(38) Barton, G.; Bray, A. J.; McKane, A. J. *Am. J. Phys.* **1990**, *58*, 751−755.
(39) Suryanarayana, D.; Weil, J. A. *J. Chem. Phys.* **1976**, *64*, 510−513.
(40) Becke, A. D.; Roussel, M. R. *Phys. Rev. A: At., Mol., Opt. Phys.* **1989**, *39*, 3761−3767.
(41) Dunning, T. H., Jr. *J. Chem. Phys.* **1989**, *90*, 1007−1023.
(42) Kendall, R. A.; Dunning, T. H., Jr.; Harrison, R. J. *J. Chem. Phys.* **1992**, *96*, 6796−6806.
(43) Woon, D. E.; Dunning, T. H., Jr. *J. Chem. Phys.* **1993**, *98*, 1358−1374.

Table 8. Hyperfine Couplings[a] in Caged (A_p) and Free (A_p^{free}) Hydrogen Atoms

	HF		B3LYP	
basis	A_p	$1 - A_p/A_p^{free}$	A_p	$1 - A_p/A_p^{free}$
3-21G*	1212.9	0.086	1136.7	0.007
6-311G**	1415.5	0.102	1358.6	0.023
DZ[b]	1309.3	0.089	1215.4	0.017
TZ[b]	1409.7	0.099	1355.0	0.025
QZ[b]	1460.1	0.094	1407.4	0.016
5Z[b]	1505.5	0.089	1460.4	0.016

[a] Hyperfine coupling in MHz. B3LYP model. [b] Augmented correlation-consistent basis sets.

yield very similar results to the corresponding Pople sets. In the calculations here, the cc-pvxz sets are further augmented with one set each of diffuse s, p, d, and f functions. The resulting sets are known as aug-cc-pvxz. The leftmost two columns of Table 8 show the results of these calculations; the remainder of the table shows results (total energy and A_p) for the isolated H atom using the same basis sets. In UHF, for the isolated H atom, the total energy steadily approaches its asymptote as the basis set is improved, and at the quintuple ζ level is within 5 ppm of its exact value, whereas at the same basis, the Fermi contact interaction still deviates from the exact or the experimental value by more than 2%. This is mainly due to the cusp description problem; decontraction of the basis, possibly supplemented by the use of a geometrical series of compact s-exponents, can further improve the Gaussian basis Hartree−Fock results to near-exactness.[47] The free atom density functional values (B3LYP, BPW91), however, *overshoot* the exact energy somewhere between the double-ζ and triple-ζ levels in the basis set space and overshoot the exact A_p between quadruple-ζ and quintuple-ζ. (The lag in the overshoot can be attributed to the same cusp problems that lead HF to underestimate A_p.)

With the convention $f = A/A_{vac}$, Dilger et al. employ the expression

$$\langle f \rangle_{n_x n_y n_z} = 1 + c_0 + c_2 \langle R^2 \rangle_{n_x n_y n_z} \tag{13}$$

to describe the dynamical effects on the coupling in the atom-cage system, with c_0 effectively representing the compression of the wave function and c_2 giving a first (quadratic) approximation to the vibrational spin delocalization effects. (Dilger et al. sometimes employed an additional c_3 term ostensibly to represent atom-cage coupling, and this yielded better results in some cases; however, deviation from the harmonic model can also be expected in any case, even in a purely rigid approximation, due to the anisotropy of the three-dimensional cage potential.)

With the temperature dependence then given by a Boltzmann average of the form

$$\langle f \rangle(T) = 1 + c_0 + c_2 \frac{\sum_{n_x n_y n_z} \left(\frac{3}{2} + N\right) \exp\left(-N\frac{h\omega}{k_B T}\right)}{\sum_{n_x n_y n_z} \exp\left(-N\frac{h\omega}{k_B T}\right)} \tag{14}$$

where $N = n_x + n_y + n_z$, the model should be isotope independent. Their global (i.e., over all isotope data) experimental fits yielded values of $c_0 = 4.6 \times 10^{-3}$ for the Q_8M_8 cage and $c_0 = 0.36 \times 10^{-3}$ for the EtT_8 cage within the uncoupled approximation. In both cases, these values are much smaller than the ones obtained here for $H@HT_8$, with Hartree−Fock yielding $c_0 \approx 9 \times 10^{-2}$ and B3LYP yielding $c_0 \approx 2 \times 10^{-2}$. In addition, the two techniques are in rather poor agreement, suggesting that a better description of the entire atom-cage system is needed before meaningful comparison with experiment is possible. (In fairness to the calculations, however, it should be pointed out that individual experimental fits to single-isotope data sets typically lead to quite different values of c_0, sometimes even of negative sign, and so the degree of error in the experimental value should probably be thought of as quite large.[36])

The hyperfine coupling of the caged atom as a function of the face-center to face-center coordinate q is shown in Figure 9b, calculated at the 3-21+G* level using the ROHF, UHF, UB3LYP, and UBPW91 methods. (Further calculations were carried out using UHF and UB3LYP with the 6-311++G** basis and using UMP2 with the 3-21+G* basis to confirm these results.) The qualitative behavior of A_p is strikingly different across these four methods and merits further discussion. In both Hartree−Fock methods, the coupling goes through a fairly sharp maximum roughly coincident with the maximum in the total energy then declines smoothly outside the cage to the free-atom value. Within the cage, however, the two methods show differences, with the unrestricted technique (seemingly irrespective of basis set size) yielding a steady increase toward the maximum, whereas the restricted method shows a plateau and a small dip over this same region. The spin contamination in the UHF wave function rises steadily in this region, though at no point is it very severe. The dip near the cage center reappears in the unrestricted MP2 method with the same basis, suggesting that the behavior of UHF may be the anomaly and the dip may be genuine. In the hybrid DFT B3LYP calculation, the peak at the energy maximum is still present, but much diminished in size, whereas within the cage there are now two prominent off-center minima, at $q \approx \pm 1.2$ Å. These minima are even more emphatic in the BPW91 calculation, and the maxima have now disappeared, to be replaced with "bumps" on the general upward gradient that now accompanies increasing q, tailing off with a small decrease on exiting the cage. The most striking consequence of this phenomenon is that c_0 is negative for this technique, taking values of −0.032 at the 3-21+G* level and −0.065 at the 6-31+G* level. (Though Roduner et al.[36] obtain positive and negative values of c_0 from their various fits, the absolute values calculated here are an order of magnitude larger.)

It is possible to recover an approximate value for c_2 from the Hartree−Fock and DFT calculations if it is assumed that both the total energy V and the hyperfine coupling constant A_p obtained in the one-dimensional scans are isotropic functions of r, the distance from the cage center. Then, within the harmonic approximation, we may write

$$V(r) = V_0 + \frac{1}{2} k r^2 \tag{15}$$

(44) Peterson, K. A.; Woon, D. E.; Dunning, T. H., Jr. *J. Chem. Phys.* **1994**, *100*, 7410−7415.
(45) Wilson, A. K.; van Mourik, T.; Dunning, T. H., Jr. *J. Mol. Struct. (THEOCHEM)* **1996**, *388*, 339−349.
(46) Davidson, E. R. *Chem. Phys. Lett.* **1996**, *260*, 514−518.
(47) Carmichael, I. *J. Phys. Chem.* **1997**, *101*, 4633−4636.

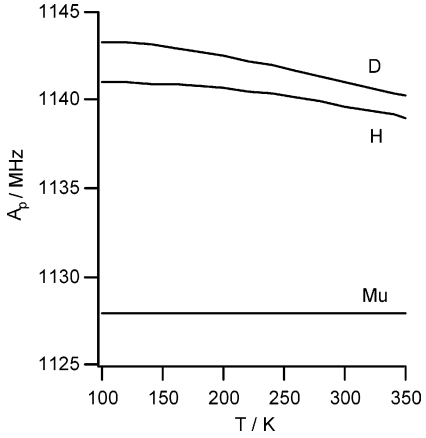

Figure 11. Temperature dependence of hydrogen isotope hyperfine coupling in rigid HT_8 computed using the isotropic model described in text.

and expand A_p (which we note is an *even* function) as

$$\begin{aligned} A_p(r) &= a_0 + \sum_i a_i r^{2i} \\ &= a_0 + \sum_i a_i (x^2 + y^2 + z^2)^i \\ &= a_0 + \sum_i a_i \sum_{\lambda+\mu+\nu=i} (i;\lambda,\mu,\nu) x^{2\lambda} y^{2\mu} z^{2\nu} \end{aligned} \tag{16}$$

where the $(i;\lambda,\mu,\nu)$ are multinomial coefficients $i!/\lambda!\mu!\nu!$. Hence, the expectation values

$$\langle A_p \rangle_{n_x n_y n_z} = \langle n_x n_y n_z | A_p | n_x n_y n_z \rangle \tag{17}$$

can be written in terms of the monomial matrix elements $K_{ij}^{(1)}$ as

$$\langle A_p \rangle_{n_x n_y n_z} = a_0 + \sum_i a_i \beta^{2i} \sum_{\lambda+\mu+\nu=i} (i;\lambda,\mu,\nu) K_{n_x n_x}^{(2\lambda)} K_{n_y n_y}^{(2\mu)} K_{n_z n_z}^{(2\nu)} \tag{18}$$

where

$$\beta = \left(\frac{\hbar}{2m\omega}\right) \tag{19}$$

and the $K_{ij}^{(1)}$ are defined according to the Hermite polynomial recursion relations.

Fitting $A_p(r)$ with terms up to r,[8] the B3LYP results in fact give reasonable agreement with the experimental temperature dependence of the H and D couplings, though clearly the absolute value of the coupling is strongly dependent on the basis set. The result obtained with the 3-21+G* basis is shown in Figure 11.

Results obtained with the 6-311++G** basis set were substantively identical subject to an upward shift of the curves by ~320 MHz. These calculations predict a flatter dependence for A'_μ than is obtained using Roduner et al.'s model. It should be noted though that because the assumption of isotropy is unwarranted by the local symmetry, a proper three-dimensional treatment might yield quite different predictions. (Kaupp explicitly considers displacements—though only up to 0.6 Å—along the (100) center to face center, (110) center to face edge, and (111) center to corner directions and finds the energy increase and hyperfine coupling constant decrease to be somewhat steeper along (110) and (111) than along (100).[31]) It is worth mentioning also that the predicted dependence is directly related to the falloff in A_p immediately on moving away from the cage center; this is much weaker in ROHF and UMP2, and accordingly, these methods predict a much smaller temperature dependence than observed experimentally (by about a factor of 10). UHF predicts an *increase* in A_p with temperature, which is quite clearly contradicted by experiment.

A version of the parameter c_2 can be obtained directly using the above approach if $A_p(r)$ is fitted using only an r^2 term. For example, with

$$\langle f \rangle_{0,0,0} = \frac{\langle A_p \rangle_{0,0,0}}{A_{p,\text{free}}} \equiv 1 + c_0 + c_2 \langle r^2 \rangle_{0,0,0} \tag{20}$$

we obtain $c_2 = -6.8 \times 10^{-3}$ Å^{-2} for the B3LYP/3-21+G* data on HT_8. However, this approach is of limited expository power as a result of the generally poor proportionality between $A_p(r)$ and $\langle r^2 \rangle$.

The experimentally observed proton hyperfine couplings indicate that the nature of the corner groups has a moderately substantial effect on the hfc of the encaged H atom; in the Roduner group's approach, this finding is embodied in c_0 values that are an order of magnitude larger for Q_8M_8 than for EtT_8. This aspect of the problem is not explored here. At the B3LYP/6-311++G** level, the small difference in A_p calculated between H@HT_8 and H@MeT_8 (1370.4 MHz vs 1358.2 MHz) cannot unequivocally be attributed to terminating group effects on wave function compression without further work.

The above vibrational averaging calculations, insofar as they purport to model the temperature-dependent hyperfine coupling, assume that the hyperfine effects originate primarily in the vibrations of the hydrogenic atom itself, largely decoupled from the motions of the cage. This is essentially the assumption made by Dilger et al.,[2] and its reasonableness is borne out by the quality of the experimental fit to the harmonic model that they obtain (and by the good match between their extracted harmonic parameters and the calculated ones). Naturally, however, it is possible that the cage vibrations also have a significant influence and, in particular, that excitation of breathing motions may lead to a larger average cage structure at high temperatures and that this may in turn lead to a diminution in the wave function compression and concomitant drop in the coupling. This would be analogous, say, to the lattice constant dependence of the temperature-dependent hyperfine coupling constant of trapped H atoms in quartz.[39,48] (Dinse, for example, finds a change in ENDOR line shape for D@EtT_8 as a function of temperature which may have such an origin.[32]) Although a detailed examination of this possibility would require sophisticated calculations not attempted here, as a rough estimate of the degree to which vibrations alter the averaged cage structure, crude molecular dynamics calculations were carried out on the HT_8 cage using the MM2 potential (after first optimizing the structure within this model) employing the program Chem3D Pro; 10 000 2-fs steps were computed at 100, 200, 300, 400, and 500 K, and the average value of the Si−Si body diagonal was calculated at each temperature.

The result is plotted in Figure 12, showing a very small increase with temperature and suggesting that cage expansion

(48) Perlson, B. D.; Weil, J. A. *J. Magn. Reson.* **1974**, *15*, 594.

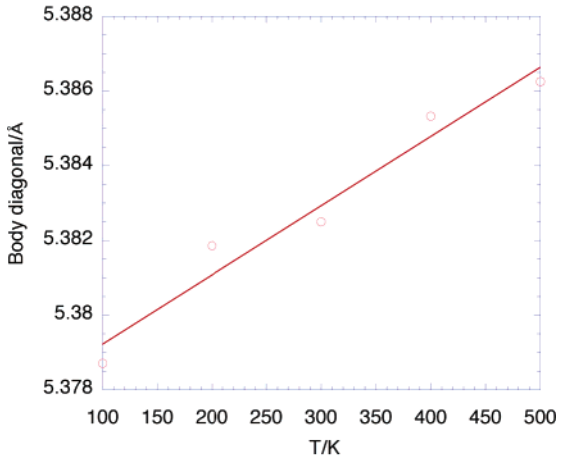

Figure 12. Si−Si body diagonal as a function of T from molecular dynamics calculations.

Table 9. Calculated[a] Harmonic Frequencies of HT_8 and $H@HT_8$

label	irrep.	HT_8[b]	HT_8[c]	$H@HT_8$[b]	HT_8[d]
ν_α	T_{1u}	415	391	414	399
ν_β	E_g	436	412	431	423
ν_γ	A_{1g}	436	437	438	456
ν_δ	T_{1u}	444	450		465
ν_ϵ	T_{1u}	575	553	572	566
ν_ζ	A_{1g}	590	573	592	566

[a] Calculated using B3LYP (in cm^{-1}). [b] 3-21+G* basis. [c] 6-31+G* basis. [d] Experimental.

may not be significant. It should be noted, though, that this calculation does not distinguish between "breathing"-type expansion and a greater incidence of distorted geometries with one long body diagonal. To calculate the effect on the hyperfine coupling *directly*, it will be necessary to carry out the dynamics using a model in which spin density and nonbonded interactions are both treated properly; this will be an interesting future project.

An alternative approach to consideration of the influence of vibration on the mechanism of detrapping is to consider the normal modes obtained by second derivative calculations at the energy minimum. Bornhauser and Calzaferri[49] have given theoretical consideration to the ring-opening vibrations of HT_8 in an attempt to assign the lines in the experimental IR, Raman, and inelastic neutron scattering spectra. They employ a simplified set of internal coordinates (describing a cubic arrangement of four-rings) and identify

$$\Gamma_{\mathrm{RO}}^{\mathrm{AR}} = A_{1g} + E_g + T_{1u} \qquad (21)$$

as the irreducible representation containing the ring breathing modes. The T_{1u} modes at 481 and 397 cm^{-1} (the frequencies are their calculated values rather than the experimental values) are then identified as the IR-active ring-opening modes of HT_8, whereas the Raman-active modes are the A_{1u} mode at 446 cm^{-1} and the E_g mode at 423 cm^{-1}. Noting that the true HT_8 system consists of a Si subsystem and an O subsystem, which will likely interact to yield somewhat more complex modes than simple "ring-opening", we tabulate a subset of relevant computed modes in Table 9.

The A_{1g} mode ν_γ is the totally symmetric breathing mode of the entire molecule, whereas ν_ζ is a mode in which the Si and O subsystems move out of phase with one another but the mode retains A_{1g} symmetry. Similarly, among the less symmetric face breathing modes, ν_ϵ is mostly a mode of the Si atoms whereas ν_β involves mostly the O atoms. The agreement with experiment improves with increased basis set size. The modes of the combined atom-cage system $H@HT_8$ are very similar to those of the bare cage, except that displacement of the H atom couples with ν_δ so that these modes can no longer be exclusively identified as ring opening. A triply degenerate T_{1u} mode at 530 cm^{-1} corresponds to a much more weakly coupled motion of the atom in the cage. This is in good agreement with a value of 522 cm^{-1} corresponding to $k = 16.2$ N m^{-1} as obtained from the one-dimensional harmonic fit to H atom displacements in the rigid cage. (Note that the interaction of cage and trapped atom modes is likely to be even qualitatively quite isotope-dependent, as the different possible H isotopic masses can move the relevant frequencies into the range of cage modes with different symmetries.) For the purpose of considering which, if any, of these modes is likely to be related to detrapping, we observe that the lowest of these modes corresponds to a temperature of about 575 K, well above the temperature at which detrapping begins in most systems. (This does not, however, exclude cage vibrations from playing some role; because the barrier-crossing is irreversible, only a small fraction of the cages would need to be vibrationally excited at any time to yield a quite substantial detrapping rate.) Also, given the foregoing geometrical arguments, it seems likely that modes affecting the oxygen 4-ring are more probably involved in the detrapping process than those primarily moving Si atoms. Substitution of the terminating H atoms with methyl groups leads to a frequency downshift (and reordering) of these ring breathing modes, with MeT_8 yielding values of 379, 389, 440, 463, 512, and 526 cm^{-1} for ν_γ, ν_α, ν_β, ν_δ, ν_ζ, and ν_ϵ, respectively. Clearly, still larger terminating groups and/or the influence of the environment (solvent, solid state) can be expected to have further effects on these modes in the general case.

Si_7Ge. Hydrogen atom trapping in the corner-substituted system $Si_7GeO_{12}H_8$ (Si_7Ge) was also studied, using the B3LYP method and the basis sets 6-31G** and 6-311G**. This molecule offers a major difference from the RT_8 species—two distinguishable trapping/detrapping transition states can be envisaged, with the H atom passing through the faces proximal (p) and distal (d) to the Ge atom, respectively. The empty cage and the filled cage have C_{3v} symmetry, but in the transition states, this is reduced to C_s. The relevant structures and energetic relationships are shown in Figure 13, and the calculated values of E_{a1}, $E_{a'1}$, E_{a11}, and $E_{a'11}$ (defined in the figure) are laid out in Table 10.

The B3LYP results are essentially independent of basis set, yielding a "p" transition state more stable than the "d" transition state by $\Delta E_{pd} \approx 34$ kJ mol^{-1}. In the UHF and UMP2 methods, this stabilization energy $\Delta E_{pd} = -7.14$ and $+9.13$ kJ mol^{-1}, respectively, but it should be noted that the geometries studied in these methods are not true stationary points (as they were obtained by optimizations using B3LYP) and likely retain structural distortion energies in excess of this rather small difference. That the B3LYP geometries are true transition states was, however, verified by second derivative calculations, which

(49) Bornhauser, P.; Calzaferri, G. *J. Phys. Chem.* **1996**, *100*, 2035−2044.

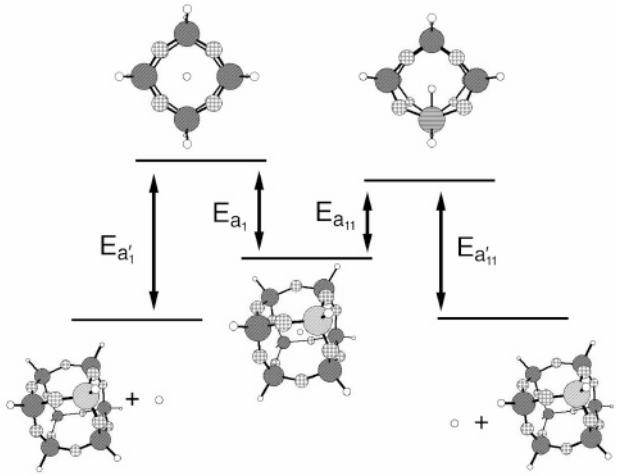

Figure 13. Structures and relative energies of the H + Si_7Ge system.

Table 10. Calculated Trapping/Detrapping Energetics[a] in H@Si_7Ge

method	E_{a1}[b]	$E_{a'1}$	E_{a11}	$E_{a'11}$	ΔE
B3LYP[c]	104	132	70.2	98.7	28.5
B3LYP[d]	108	136	71.4	103	30.7
UHF[c]	158	218	165	225	59.3
UMP2[c]	131	171	122	162	40.0

[a] Energies in kJ mol^{-1} at B3LYP geometry. [b] Parameters defined in Figure 13. [c] 6-31G* basis set. [d] 6-311G** basis set.

revealed exactly one imaginary mode of A′ symmetry in each case, corresponding to the H atom trapping/detrapping coordinate.

Structurally, the bare cage is only slightly distorted with respect to HT_8, to accommodate the somewhat longer Ge−O bonds (1.767 Å as compared to 1.642 Å for Si−O). (These and all subsequent geometrical comments refer to the B3LYP/6-311G** calculations.) The Ge−O−Si bond angle is slightly smaller than the Si−O−Si angle, at about 146° as opposed to 150°. Encapsulation of an H atom in the cage makes very little difference to the geometry, with the framework bonds stretching by an average of 0.002 Å. The caged atom lies along the Ge−Si body diagonal, with $r_{Ge-H} = 2.745$ Å and $r_{Si-H} = 2.845$ Å, probably indicating a greater flexibility of Ge to rearrange its electronic density distribution to minimize repulsive interactions. The two transition states, however, are structurally much more interesting. Whereas the "d" state resembles the transition states in HT_8 and MeT_8, with the H atom passing roughly through the face center (the Si−H distances at the TS are 2.297, 2.269, 2.269, and 2.267 Å, with H slightly displaced away from the Ge side of the cage) and very little distortion at Ge, the "p" state exhibits a highly distorted structure around Ge, in which the Ge atom has essentially changed its coordination environment to accommodate the passage of the H atom through the Si_3Ge face; the O−Ge−O angle opens up from 109° (in H@Si_7-Ge) to 135°, and the H−Ge distance is only 1.680 Å (compared to 1.513 Å for the distance to the bonded H atom on the cage exterior). This flexibility to distort yields an energy saving of ∼34 kJ mol^{-1} with respect to the other TS.

The consequences for detrapping behavior of the existence of two distinct transition states are not straightforward to predict, as they may depend to some extent on the changed vibrational behavior of the reduced-symmetry cage. However, it is clear that the *net* kinetic parameters for detrapping will most likely reflect an average over the two channels, leading to a lower overall barrier than in the RT_8 species; this is indeed reflected in the experimental data, though not to the extent predicted by the B3LYP method.

The lowered symmetry of the system leads to vibrational modes that are qualitatively different from those of the all-Si cages. At the 6-311G** level, modes at 388 (×2), 401, 419 (×2), 423, 445, 446, and 448 cm^{-1} all contain some degree of ring opening in either or both of the SiGe and O subsystems. (In fact, the distinction between subsystems is not so clean as in the all-Si cases.) These modes are all unsymmetrical with respect to the Ge-containing and non-Ge-containing faces, and in particular, the O-atom displacement associated with the Ge-containing faces in the 388 cm^{-1} modes is greater than that associated with the non-Ge-containing faces and consists of a pushing apart of two of the oxygens associated with Ge while the third remains relatively unmoved—this may be directly connected to the mechanism of H-atom escape and account for the lower temperature at which it occurs in this species. As was found with the all-Si species, there is likely to be a dependence of the vibrational mode frequencies on the terminating groups chosen, and here it is additionally to be noted that Si and Ge possess different attached groups in the system studied experimentally.

The Fermi contact coupling constants obtained in H@Si_7Ge were $A_p \approx 1338.95$ (B3LYP/6-31G*), 1432.05 (UHF/6-31G*), 1382.09 (UMP2/6-31G*), and 1343.32 MHz (B3LYP/6-311G**). The 6-311G** value compares with $A_p \approx 1327.80$ MHz for free H, yielding a c_0 of ∼0.01, somewhat smaller than those in H@HT_8. Of note also is the fact that because the O_h symmetry has been lost, there is now a finite dipolar contribution to the hyperfine coupling. The principal axis components of this coupling are calculated to be (in MHz) $(D_{xx},D_{yy},D_{zz}) =$ (−0.281,−0.262,0.543) (B3LYP/6-31G*), (−0.287,−0.271,0.558) (B3LYP/6-311G**), (−0.223,−0.196,0.419) (UHF/6-31G*), and (−0.226,−0.201,0.427) (UMP2/6-31G*). Note that only the B3LYP results are at properly optimized geometries. Deviations from axial symmetry are at the level of numerical "noise" due to lack of strict enforcement of symmetry constraints during the calculations. Muon spectroscopy methods have shown themselves capable of revealing dipolar tensor anisotropies in C_{70} at low temperatures,[1,50,51] and it would be of interest to pursue similar studies of the present system.

Si Superhyperfine Couplings. To extract quantitatively accurate ^{29}Si superhyperfine couplings from ab initio calculations is a much more serious challenge than the calculation of ^1H couplings due to the influence of polarization effects between the core (1s), inner valence (2s, 2p), and outer valence (3s, 3p) electronic shells; the net coupling will consist of a direct component from the hydrogen 1s density together with a polarization component which will be a sum of possibly large terms most likely of alternating sign. Additionally, traditional Gaussian basis sets are relatively inflexible in their description of the core region, making them intrinsically rather inappropriate

(50) Macrae, R. M.; Prassides, K.; Thomas, I. M.; Roduner, E.; Niedermayer, C.; Binninger, U.; Bernhard, C.; Hofer, A.; Reid, I. D. *J. Phys. Chem.* **1994**, *98*, 12133−12141.
(51) Binninger, U.; Bernhard, C.; Hofer, A.; Niedermayer, C.; Recknagel, E.; Erxmeyer, J.; Weidinger, A. *Phys. Rev. B: Condens. Matter Mater. Phys.* **1995**, *51*, 14867−14873.

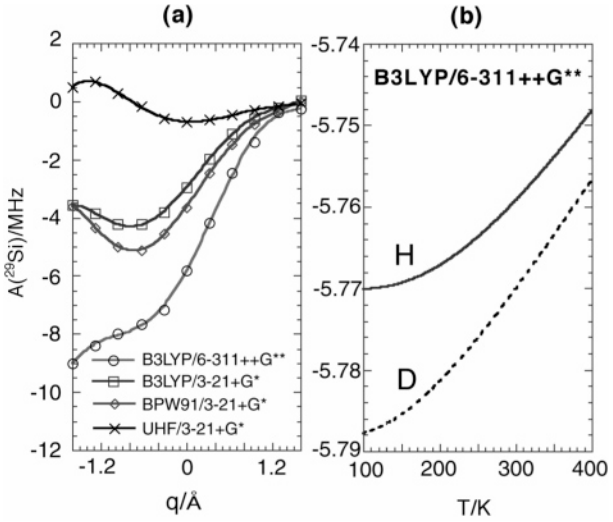

Figure 14. (a) Calculated ^{29}Si superhyperfine coupling in H@HT$_8$ vs intra-cage H displacement; (b) calculated temperature dependence of ^{29}Si coupling.

for the calculations of Fermi contact couplings in heavy atoms. Although the present level of theory is not adequate to describe these quantitatively, we can use our data to demonstrate the principle of how a calculation of the temperature-dependent coupling might proceed.

The dependence of the ^{29}Si coupling of one corner silicon atom upon rigid displacement of H in the manner described above is shown in Figure 14a. (The positive direction in the figure corresponds to increasing H−Si distance.)

Clearly four Si atoms show curves identical to this, whereas the other four have dependencies equivalent to the reflection of this figure in the *y*-axis. The first point to note is that as the coupling is not an even function of the displacement the isotropic model cannot be used. The values given by the UHF calculation are qualitatively rather different from those given by density functional methods, whereas the DFT results show common features and, for a given basis set, considerable similarity between the two methods (B3LYP and BPW91) used. The couplings are of negative sign because of the sign of the ^{29}Si gyromagnetic ratio—they correspond to positive spin density at the ^{29}Si nucleus, indicating that the dominant factor is most likely the direct contribution from the hydrogenic 1s function. This tails off to near zero when the H atom is at the far extreme of the cage from the Si atom in question. As H nears the Si four-ring the absolute value of the coupling increases, and in the small basis calculations passes through a maximum that is absent in calculations with the larger basis.

We employ a simple model to simulate the temperature-dependent coupling. The H atom is assumed to move in one of three orthogonal cylindrical channels in the face-center to face-center directions, where it experiences a pseudo-one-dimensional potential that we approximate, as before, with a harmonic potential. The coupling is then expanded as a polynomial in the displacement coordinate, and the coupling expectation values are generated in terms of the diagonal matrix elements of the powers of the displacement, i.e.

$$\langle n|A_{\mathrm{Si}}|n\rangle = a_0 + \sum_i a_i \langle n|q^i|n\rangle \qquad (22)$$

These matrix elements are again expressed in terms of the monomial matrix elements, more simply this time.

$$\langle A_{\mathrm{Si}}\rangle_n = a_0 + \sum_i a_i \beta^i K_n^{(i)} \qquad (23)$$

Finally, the temperature dependence is obtained by Boltzmann averaging. The temperature-dependent coupling obtained using B3LYP/6-311++G** is shown in Figure 14b. Given that the experimental coupling is in fact negative, the computed values reproduce the qualitative behavior rather well. The coupling has a larger absolute value in the D@HT$_8$ case than in the H@HT$_8$ case and has a steeper slope. The numerical values of the computed couplings with this basis are slightly too large, and the temperature dependence is, in both cases, too flat. That qualitative agreement can be obtained with such a crude model is, however, striking. The B3LYP/3-21+G* data and the BPW91/3-21+G* data give qualitatively similar behavior but underestimate the coupling by almost a factor of 2. It will be of interest in the future to explore the effect upon the ^{29}Si coupling of using an appropriate large, well-balanced basis set and averaging over a more realistic anisotropic three-dimensional potential and property surface.

Concluding Remarks

From careful measurements of the thermally induced detrapping of hydrogen atoms from different octasilsesquioxanes, we were able to provide more accurate estimates of the detrapping activation energy E_A. It was shown that variation of cage substituents has little influence upon E_A. Nor is the detrapping process influenced by radicals or peroxyl groups present in the irradiated specimen. There is, however, a measurable difference in the activation parameter E_A for detrapping hydrogen as compared to deuterium. This effect is due to the difference in zero-point vibrational energies of H and D. One-dimensional calculations of the potential inside the cage showed that the effect of cage relaxation on the detrapping energetics occurs mostly when the H/D atom is near the plane of the oxygens, suggesting that rigid studies would be a sufficient zero-order approach to the intra-cage potential and properties. Calculations of this kind allowed the zero-point energy difference to be estimated, giving reasonable agreement with experiment. The qualitative features of the variation of the hyperfine coupling constant of H moving within the cage were found to be dependent on the computational technique employed; use of the B3LYP values together with a simple isotropic model of the potential and hyperfine coupling gave good agreement with the experimentally observed temperature dependence.[2,36] Hydrogen was found experimentally to leave germasilsesquioxane cages with a lower barrier than for octasilsesquioxanes; quantum chemical calculations suggest that this behavior is related to a significant stabilization of the transition state in which H passes through the Ge-containing face. The temperature dependence of the ^{29}Si superhyperfine coupling constants was measured experimentally, showing an H/D isotope dependent slope and low-temperature limit. Although the quantum chemical models used should not be expected to yield quantitatively meaningful ^{29}Si couplings, the B3LYP values analyzed within a simple dynamical model succeeded in reproducing the qualitative features of the data.

Acknowledgment. The support for M.P. by the Deutsche Forschungsgemeinschaft is gratefully acknowledged. Further acknowledgments are due to Prof. K.-P. Dinse (TU Darmstadt) and his group for fruitful discussions in Darmstadt as well as for generously making the VTC available to us. Use of the supercomputing facilities at NERSC in the early stages of this project is gratefully acknowledged. The research described herein was supported by the Basic Energy Sciences at the Department of Energy. This is Contribution No. 4617 from the Notre Dame Radiation Laboratory.

Supporting Information Available: Cartesian coordinates and total energies of optimized structures; complete ref 19. This material is available free of charge via the Internet at http://pubs.acs.org.

JA055177D